# Synthesis of Nanoscale Nd-Doped Ceria *Via* Urea-Formaldehyde Combustion Method

M. BISWAS and S. BANDYOPADHYAY

Nanocrystalline neodymium-doped ceria solid solutions with $Nd^{3+}$ concentrations varying from 4 to 20 mol pct have been synthesized by gel combustion method, using urea-formaldehyde as fuel for Nd doping. The combustion reaction is explained through differential scanning calorimetry (DSC)-differential thermogravimetric analysis (TGA), whereas the synthesized materials are characterized through X-ray diffractometry (XRD), field-emission scanning electron microscopy (FESEM), and transmission electron microscopy (TEM). The phase obtained from the exothermic reaction contains Nd-substituted $CeO_2$. The deviation of the lattice parameter from Vegard's law and the decrease in crystallite size with dopant concentration has been explained. The as-synthesized particles are largely nanoporous single crystallites, existing in loosely held spherical-shaped agglomerates. The size of the agglomerates increases with increasing dopant content. High-resolution TEM (HRTEM) reveals the fact that the unit cells are strained.

DOI: 10.1007/s11661-013-1863-z


## I. INTRODUCTION

BECAUSE of the isotropic structure, cerium oxide is a transparent ceramic suitable for applications in different optical and optoelectronic devices.[1] It can withstand high temperatures and harsh conditions during processing without losing its optical properties.[2] The material has found many other potential applications in some fields such as gas sensors,[3] absorbents of electromagnetic wave in ultraviolet range,[4] electrolyte and anode materials in solid oxide fuel cells,[5] and oxidation-resistant coatings for high-temperature application.[6] The nanocrystalline materials display a quantum confinement effect evidenced through blue shift in the ultraviolet absorption spectrum,[4] lattice expansion,[7] and shifting and broadening in Raman allowed modes.[8] Recently, the material has also become a potential candidate in the field of catalytic bed, specifically due to its oxygen absorption and release capabilities.[9] These capabilities result from the ability of cerium to change valance state from 4+ to 3+, while existing large octahedral void allows the oxygen movement inside the structure.[10,11] In addition to these intrinsic properties, the oxygen absorption and desorption characteristics can be maneuvered extrinsically through (1) the addition of lower valent cations into the sites of $Ce^{4+}$ and thereby (2) the simultaneous creation of oxygen vacancy in structure to maintain charge neutrality. Investigations with rare-earth oxides are available in this regard.[12–14] Nanocrystalline powders have been prepared by various routes such as the conventional solid-state reaction method,[15] carbonate coprecipitation,[16] oxalate coprecipitation,[17] self-propagating room-temperature synthesis,[18] microemulsion process,[13] *etc*. The gel combustion route can be regarded as another attractive alternative for nanosized material preparation.[19] The attractive feature of this process lies in an intimate blending among the fuel or complexing agents (*e.g*., glycine, citric acid, urea, L-alanine, *etc*.) and oxidizer in an aqueous medium.[20–23] The mixture gets ignited with subsequent self-sustaining exothermic redox reaction between the fuel and the oxidant. The rapid evolution of a large volume of gases due to the exothermic (combustion) reaction dissipates the heat of combustion, thereby limiting the increase of temperature that, in turn, reduces the possibility of local partial sintering among the primary particles. In this synthesis route, the type and amount of fuel play significant role in determining particle morphology.

Urea formaldehyde (UF) as fuel has shown interesting results in synthesizing nanocrystalline yttria -doped ceria[24] and lanthanum strontium manganate powders.[25] In the current work, the possibility of preparing nanocrystalline ceria by the combustion technique using UF as fuel for doping of $NdO_{1.5}$ is explored. The primary particles thus formed were characterized by X-ray diffractometry (XRD), transmission electron microscopy (TEM), and field emission scanning electron microscopy (FESEM). The nature of combustion propagation, changes in cell parameters, and grain morphology have been discussed.

## II. EXPERIMENTAL

Ceria doped with neodymium oxide with concentration varying between 4 and 20 mol pct (with the step size of 4 mol pct) have been prepared using Ce(III)nitrate hexahydrate (99.9 pct; Strem Chemicals, Newburyport, MA), neodymium oxide (99.9 pct; Indian Rare Earth Ltd.,

M. BISWAS, Research Associate, and S. BANDYOPADHYAY, Chief Scientist, are with the CSIR-Central Glass & Ceramic Research Institute, Kolkata 700 032, India. Contact e-mail: sbando@cgcri.res.in
Manuscript submitted October 9, 2012.



Published online: 09 July 2013

Mumbai, India), urea (Merck, Whitehouse Station, NJ), solution of formaldehyde (37 pct (w/v), Merck), nitric acid (Merck), and ammonia solution (Merck) of LR grade. At the first step, neodymium nitrate was prepared by reacting neodymium oxide with nitric acid. Next, urea was hydroxymethylolated with the addition of formaldehyde solution and adjusted to pH 8.5 using an ammonia solution.[26,27] The ratio of urea to formaldehyde was maintained as 1:4. The resultant solution was kept undisturbed for 24 hours. The following reaction takes place[27]:

$$\begin{aligned} &NH_2 - CO - NH_2 + HCHO \rightarrow HO - H_2C \\ &- NH - CO - NH - CH_2 - OH \end{aligned} \quad [1]$$

This step is carried out in basic pH region for methylolation reaction without condensation.[27] The second step consists of addition of metal nitrates in stoichiometric amount followed by addition of urea. The ratio of urea to formaldehyde was kept as 1:2. Throughout the investigation, the metal nitrates to urea concentration was also taken in the same ratio; a similar ratio has also been used by Prabhakaran *et al.*[25] The pH of the solution goes down to the acidic range due to the presence of nitrates. In this stage, a condensation reaction takes place and urea-formaldehyde resin is formed. The resin was dried at 383 K (110 °C) to convert the liquid resin to a solid gel. The solid gel was ignited to form the product. A light-green colored powder was produced.

The combustion characteristics and mass loss spectrum of the gel was studied by differential scanning calorimetry (DSC) along with differential thermogravimetric analysis (TGA) (Netzsch, Selb, Germany; Models STA409C & STA449C) at a heating rate of 10 K/min (10 °C/min) in the temperature range of 308 K to 1073 K (35 °C to 800 °C) in air atmosphere.

The phase formation of the as-combusted powder was studied by XRD (Philips PW-1730; Philips, Almelo, the Netherlands) using Cu K$\alpha$ radiation (1.5406 Å) in the angular region of $2\theta$ to be 20 to 80 deg. The peak positions were corrected employing the following steps: K$\alpha_2$ stripping, background determination, peak searching, smoothening, and fitting profile. For each composition, eight peaks were taken into account after the corrections and lattice parameters were calculated following Cohen's method.[28] The two working equations of Cohen's method are presented below as follows:

$$\sum \alpha_1 \sin^2\theta = C\sum \alpha_1^2 + D\sum \alpha_1 \sin^2 2\theta \quad [2]$$

$$\sum \sin^2 2\theta * \sin^2\theta = C\sum \alpha_1 \sin^2 2\theta + D\sum \sin^4 2\theta \quad [3]$$

where

$$C = \frac{\lambda^2}{4a_o^2} \quad [4]$$

$$\alpha_1 = (h^2 + k^2 + l^2) \quad [5]$$

The experimental values of $\sin^2\theta$, $\alpha_1$, and $\sin^2 2\theta$ of all the peaks were individually calculated and substituted in Eqs. [2] and [3] for eight different peaks of each composition. Individual peak indices were used for the respective calculations of constant $\alpha_1$. These give eight sets of equations (one set contains two equations) with unknown constants of $C$ and $D$ for each composition. The least square method has been employed for these eight sets of equations to calculate the value of $C$, which is used to determine the lattice parameter $a_o$ with known value of $\lambda$ (1.5406 Å in the current experiment) following the relation given in Eq. [4].

The unit cell volume and density has also been calculated by using lattice parameter and molecular weight calculation. Fluorite-type ceria possess a face-centered cubic structure. As one unit cell in this case contains four formulae units and one mole ceria powder contains $6.023 \times 10^{23}$ numbers (Avogadro's number) of molecule, the theoretical density is calculated as follows:

$$X\text{-}ray\ density = \frac{4 \times molecular\ weight}{6.023 \times 10^{23} \times volume\ of\ unitcell} \quad [6]$$

The crystallite sizes for all the compositions were determined using Scherrer relation: $D = 0.94\lambda/\beta\cos\theta$, where $D$ is the crystallite size, $\lambda$ is the wavelength of CuK$\alpha$ radiation (1.5406 Å), $\beta$ is full width at half maxima of the broadening of the diffraction line, and $\theta$ is half the angle of diffraction.

The powder morphology was evaluated both through TEM (TECNAI G2 30ST; FEI Company, Hillsboro, OR) and FESEM (Supra 35VP; Carl Zeiss, Oberkochen, Germany). The selected-area electron diffraction (SAED, an integral part of the TEM instrument) is obtained by operating the microscope in the diffraction mode with an aperture of 10 micron from a selected area of 150 nm diameter.

## III. RESULTS AND DISCUSSION

### A. *DSC-TGA Study*

Figure 1(a) describes the way the combustion reaction of UF gel containing metal ions proceeds. Figure 1(b) represents thermogravimetry along with its rate curve. After heating, UF polymer at the first stage undergoes a cross-linking reaction in the temperature range of 373 K to 473 K (100 °C to 200 °C), and then decomposes to $CO_2$, $H_2O$, $NH_3$, and amines at temperatures from 473 K to 573 K (200 °C to 300 °C) with the formation of an intermediate stable structure. The stable structure ultimately decomposes completely between 673 K and 873 K (400 °C and 600 °C).[29] In the current experiment, two consecutive exothermic peaks with corresponding weight losses and a single exothermic peak with no weight loss have been found. The initial fall in TG curve along with a small change in the DSC curve at around 373 K (100 °C) may be attributed to the water loss associated with gel. The weight loss up to around 497 K (224 °C) corresponds to cross-linking reaction and may be attributed to the decomposition of the cross-linked structure with the evolution of $CO_2$,

$H_2O$, $NH_3$, and amines.[29] The peak in the rate curve originated out of a strong exothermic peak in DSC along with a maximum weight loss of 63.16 pct that occurred at 524 K (251 °C), may be the dual representation of the decomposition of intermediate stable structure and of the combustion reaction. The gel was observed to produce a self-sustained flame when it was kept in an oven at 523 K (250 °C). It is evident that this is the temperature for a vigorous combustion reaction of a Nd-doped ceria-containing nitrate oxidant system. One observation is that the combustion of urea-formaldehyde polymer without metal cation takes place at around 673 K to 873 K (400 °C to 600 °C).[29] The combustion temperature is brought down by the metal cation and is dependent on the specific cation, *viz*., yttria-doped ceria and lanthanum strontium manganate being 498 K (225 °C) and 623 K to 723 K (350 °C to 450 °C), respectively.[24,25] The exothermic peak [587 K (314 °C)], which is observed without corresponding weight loss, may be attributed to the crystallization of Nd-doped ceria. The effect of relative concentrations of $Nd^{3+}$ to $Ce^{4+}$ on the combustion temperature has been studied. Although the nature of combustion reaction is same, a shift in the temperatures for cross-linking reaction, a structural decomposition reaction, and crystallization has been observed (Figure 1(c)). Combustion occurs at higher temperature with larger extent of heat evolution (comparative area in the curve) for increasing concentration of dopant.

## B. *XRD Study*

Figure 2 shows an indexed XRD plot of as-synthesized ceria powders. The XRD pattern shows the powder to be crystalline, which indicates that the heat generated during a self-sustained combustion reaction is sufficient for crystallization. Therefore, this synthesis route does not require an additional calcination step.

All the XRD peaks have been processed following Cohen's method[28] and are compared with standard JCPDS values (file no. 81-0792). The peaks of $Nd_2O_3$ both in hexagonal and cubic structures are absent. Therefore, it is evident that $Nd^{3+}$ has entered the ceria lattices; *i.e*., complete solid solutions have formed. It is observed also that dopant addition shifted the peaks to the lower diffractions angles and thereby lengthened the lattice parameters.

The detailed calculation of peak positions (Table I) revealed that lattice parameter of the powders increased with increasing concentration of $Nd^{3+}$ where substitution of larger $Nd^{3+}$ (1.12Å) took place in the sites of $Ce^{4+}$ (1.01Å)[30]; the trend being presented in Figure 3(a). However, it is observed that both positive and negative deviations from Vegard's law producing an "S"-shaped pattern occurred in this system. The observation is similar to some covalent pseudobinary semiconductor alloys where the physical origin of the anomalous S-shaped violation of Vegard's law is attributed to the covalent bond-bending forces.[31] In such cases, for a small level of substitution, the bonds around

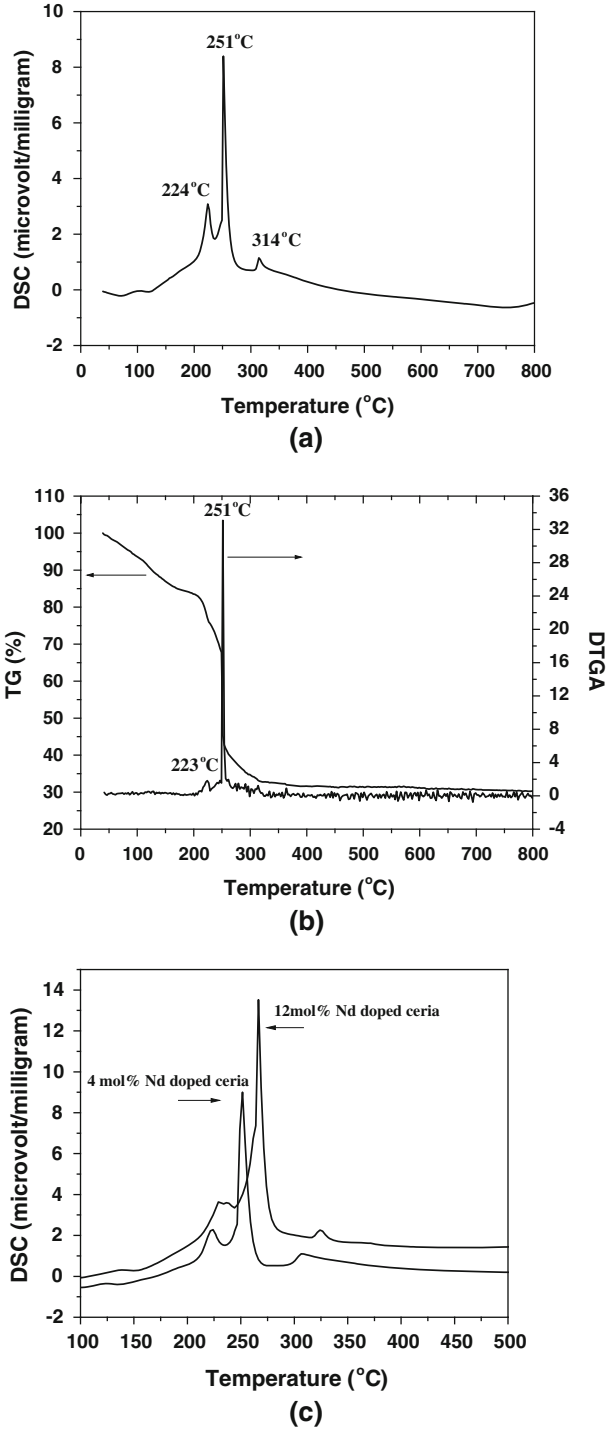


Fig. 1—(*a*) DSC plot of composition with 8 mol pct substitution of $NdO_{1.5}$ for $CeO_2$. (*b*) TG-DTGA plot of composition with 8 mol pct substitution of $NdO_{1.5}$ for $CeO_2$. (*c*) Comparative plot of DSC.

few substituted large sized ions tend to expand, which in turn induces changes of the bond angles at neighbor ions. The bond-bending forces of the host lattice, when sufficiently large, resist any distortion of angles and, thus, prevent the bonds around the substituted ions

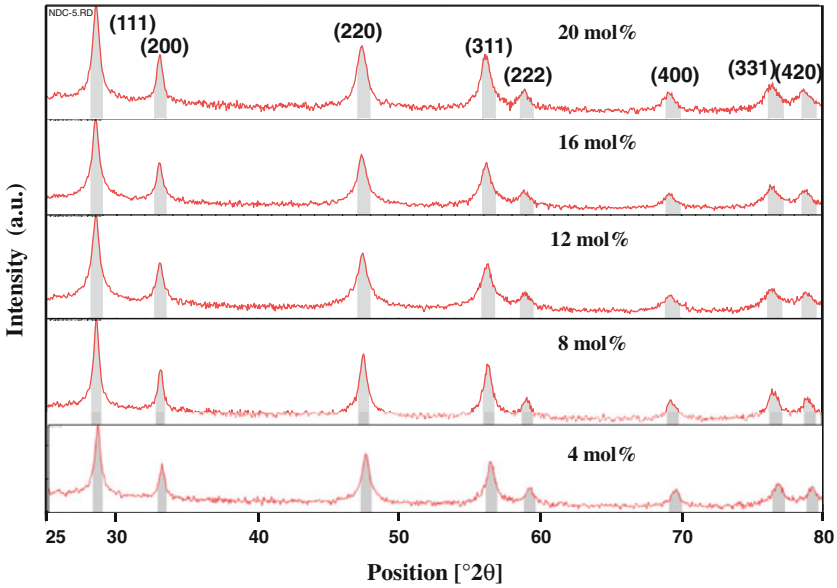


Fig. 2—XRD plots of 4 to 20 mol pct $NdO_{1.5}$ substitution.

from expanding, so that the average lattice parameter of the alloy is smaller than Vegard's value. The reverse phenomenon takes place as the substitution concentration is higher.

Figure 3(b) describes the dependence of molecular weight and theoretical density on $Nd^{3+}$ concentration. Molecular weight decreases linearly with increasing concentration of $Nd^{3+}$. Because the lattice parameter does not show any linear relationship with the concentration of $Nd^{3+}$, a similar effect is also expected for unit cell volume. Hence, the nonlinear nature of theoretical density with dopant concentration may be explained through the combined effect of molecular weight and volume (Figure 3(b)).

A decreasing trend has been observed in crystallite size with increasing $Nd^{3+}$ concentration (Figure 4). The fact may be explained through the light of recent studies[32,33] on La-doped ceria, which showed that the formation of an oxygen vacancy results in the appearance of a reduced $Ce^{3+}$ cation and a compensated oxygen hole. After oxygen vacancy formation,[33] scanning tunnelling microscopy and spectroscopy along with calculation for density function theory (DFT) showed that two excess electrons remain on (111) planes of ceria that induces negative surface charges. This negative surface should repel anions, and the tendency becomes more effective at higher substitution level of $Nd^{3+}$. At a larger concentration of the dopant, it may therefore be assumed that crystal growth gets resisted due to the repulsion between the like charges, resulting in smaller crystallite size. A similar view is presented in another study made on an analogous fluorite-type system ($NaYF_4$) that has undergone experimentation to find out the influence of dopant on the crystallite growth.[34] It was shown through DFT calculation that the substitution of $Y^{3+}$ by $Gd^{3+}$ increases electronic charge density on the crystal surface, which hindered the diffusion of negatively charged $F^-$ ions toward crystal surface due to charge repulsion.

### C. *FESEM Observation*

Figure 5 represents the typical morphological features of 20 mol pct $Nd^{3+}$ containing ceria. The general features along the entire compositional range under study (not shown) reveal that all the particles are in the average range of 50 to 100 nm. The morphology shows that they are, in general, spherical in nature with loss of symmetry in feature toward higher doping. Agglomeration was commonly seen and was also observed to increase with increasing concentration of $Nd^{3+}$. Agglomeration refers to the adhesion of particles or crystals either by Van der Waals forces of attraction[35] or by collision with each other.[36] If the residence time of the generated particles in the combustion flame is long enough to make contact among the particles or the temperature is high enough to produce a low level of sintering, then agglomeration is favored.[36] Figure 1(c) may be referred back in this context once again where we have seen that the higher concentration level of dopants shifts the combustion flame temperature toward the higher side and the heat evolution is also high. This might induce kinetic acceleration in the rate of conversion reactions. It may therefore be assumed that higher doping produces more particles and hence higher agglomeration.

### D. *TEM Observation*

One notable feature is that the agglomeration is weak in all cases, and a gentle grinding in agate mortar and pestle produces free particles with distinct features and is considered for TEM study. Figure 6 shows the images under TEM where a wide range of particle size

**Table I. Required Parameters to Calculate Lattice Parameter, $a_o$**

| Composition | 2$\theta$ Deg (Processed) | 2$\theta$ Deg (JCPDS File No. 81-0792) | ($h$ $k$ $l$) | ($h^2 + k^2 + l^2$), $\alpha$ | $C$, Solving Eqs. [2] and [3] by Least Square Method | $a_o$ (Å) Eq. [4] |
|---|---|---|---|---|---|---|
| $Ce_{0.96}Nd_{0.04}O_{1.98}$ | | | | | | |
| | 28.5542 | 28.542 | 111 | 3 | 0.020261 | 5.4116 |
| | 33.0736 | 33.075 | 200 | 4 | | |
| | 47.4708 | 47.475 | 220 | 8 | | |
| | 56.3165 | 56.332 | 311 | 11 | | |
| | 59.0783 | 59.078 | 222 | 12 | | |
| | 69.3835 | 69.401 | 400 | 16 | | |
| | 76.6674 | 76.685 | 331 | 19 | | |
| | 79.0601 | 79.060 | 420 | 20 | | |
| $Ce_{0.92}Nd_{0.08}O_{1.96}$ | | | | | | |
| | 28.5578 | 28.542 | 111 | 3 | 0.020055 | 5.4394 |
| | 33.0833 | 33.075 | 200 | 4 | | |
| | 47.4431 | 47.475 | 220 | 8 | | |
| | 56.283 | 56.332 | 311 | 11 | | |
| | 59.0368 | 59.078 | 222 | 12 | | |
| | 69.2734 | 69.401 | 400 | 16 | | |
| | 76.5023 | 76.685 | 331 | 19 | | |
| | 78.9168 | 79.060 | 420 | 20 | | |
| $Ce_{0.88}Nd_{0.12}O_{1.94}$ | | | | | | |
| | 28.5202 | 28.542 | 111 | 3 | 0.019924 | 5.4433 |
| | 33.039 | 33.075 | 200 | 4 | | |
| | 47.3856 | 47.475 | 220 | 8 | | |
| | 56.216 | 56.332 | 311 | 11 | | |
| | 58.9458 | 59.078 | 222 | 12 | | |
| | 69.2116 | 69.401 | 400 | 16 | | |
| | 76.3902 | 76.685 | 331 | 19 | | |
| | 78.8225 | 79.060 | 420 | 20 | | |
| $Ce_{0.84}Nd_{0.16}O_{1.92}$ | | | | | | |
| | 28.4533 | 28.542 | 111 | 3 | 0.020039 | 5.4415 |
| | 32.9611 | 33.075 | 200 | 4 | | |
| | 47.2925 | 47.475 | 220 | 8 | | |
| | 56.1037 | 56.332 | 311 | 11 | | |
| | 58.8082 | 59.078 | 222 | 12 | | |
| | 69.0725 | 69.401 | 400 | 16 | | |
| | 76.3016 | 76.685 | 331 | 19 | | |
| | 78.6639 | 79.060 | 420 | 20 | | |
| $Ce_{0.8}Nd_{0.2}O_{1.9}$ | | | | | | |
| | 28.4848 | 28.542 | 111 | 3 | 0.019959 | 5.4524 |
| | 32.9786 | 33.075 | 200 | 4 | | |
| | 47.2833 | 47.475 | 220 | 8 | | |
| | 56.0785 | 56.332 | 311 | 11 | | |
| | 58.8166 | 59.078 | 222 | 12 | | |
| | 69.042 | 69.401 | 400 | 16 | | |
| | 76.2938 | 76.685 | 331 | 19 | | |
| | 78.5874 | 79.060 | 420 | 20 | | |

distribution is observed. The smallest particles are in the range of 10 to 25 nm with average particle sizes around 80 to 100 nm. The micrograph also shows that the particles are porous. The diffraction pattern and high-resolution micrograph were taken using an intense electron beam concentrated on a single particle (Figure 7(a)) of 110 nm particle diameter, shown in Figures 7(b) and (c), respectively. The SAED pattern indicates that the particle is single crystalline; this fact has also been supported by high-resolution (HR) micrograph.

Indexing of the SAED pattern was carried out to find the lattice of the crystal structure with specific attention toward the presence of possible lattice distortion.[37,38] Based on the measured angle (60 deg) between the planes (111) with (420) and (422), the primary set of planes were obtained to be $(\bar{1}11)$ and $(\bar{2}42)$. The remaining spots were indexed using the addition rule of vectors (Figure 7(b)). The calculated lattice parameter values are 5.69 and 5.5242 Å, respectively. This difference between these measured values with those obtained from XRD data is an indication for the

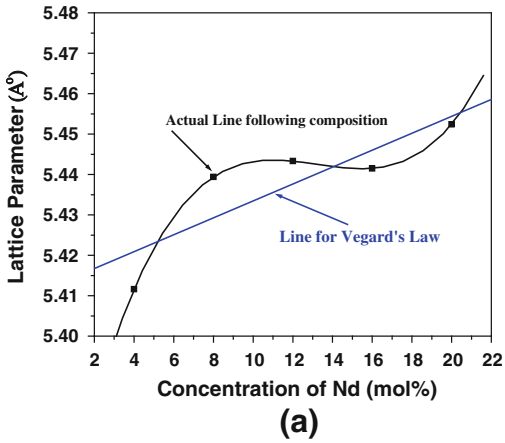


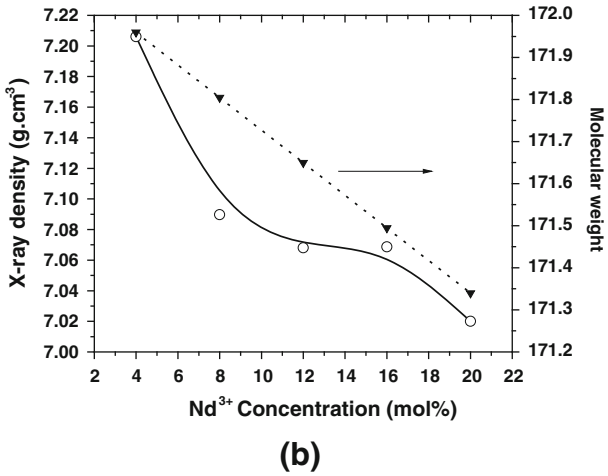


Fig. 3—(*a*) Variation of lattice parameter with $Nd^{3+}$ concentration. (*b*) Variation of theoretical density and molecular weight with $Nd3^{+}$ concentration.

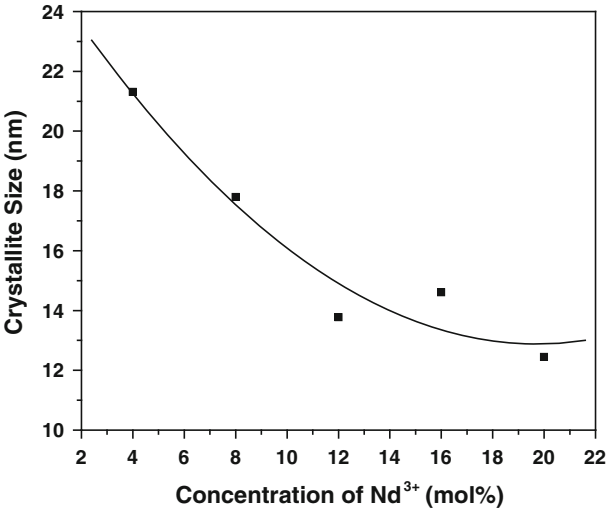


Fig. 4—Plot of crystallite size with $Nd^{3+}$ concentration.

existence of a high magnitude of lattice distortions involved in these crystals. Distortion may be attributed to the insertion of spacious $Nd^{3+}$ (1.12 Å) ion along with corresponding replacement of spacious $Ce^{3+}$

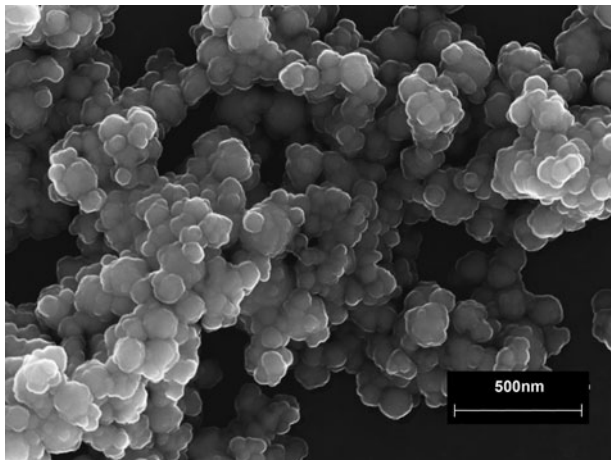


Fig. 5—Particle size distribution of 20 mol pct $NdO_{1.5}$ substituted $CeO_2$ under FESEM.

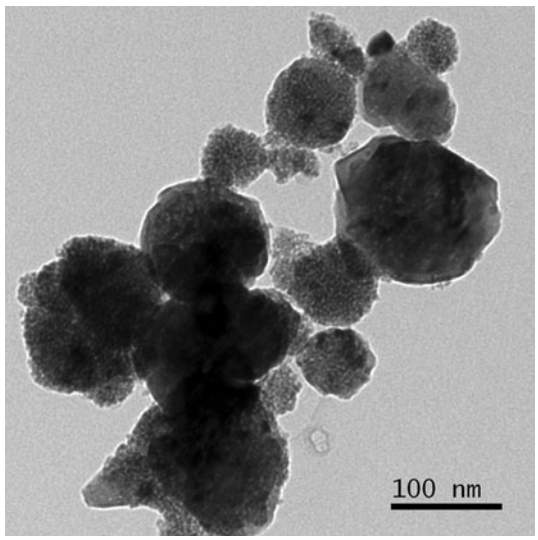


Fig. 6—TEM image of 12 mol pct Nd-doped $CeO_2$ showing particles size distribution.

(1.15 Å) ion in the $Ce^{4+}$ (1.02 Å) host lattice. Although the open configuration created by the existence of two $Ce^{3+}$ ions for one $O^{2-}$ ion in different coordination sphere around the defect tries to relax lattice strain,[33,39] it is evident that the substitutions in this case have introduced some residual strains in the unit cell. A systematic absence of some lattice points that are neither all odd nor all even was observed in the indexed SAED pattern. According to the structure factor rule of Bravais lattices, this systematic absence proves that the lattice is face centred cubic.[37,38]

The peaks in energy-dispersive X-ray spectroscopic (EDX) pattern (Figure 7(d)) show carbon (from substrate) and copper (from grids) along with peaks generated by the elements cerium, neodymium, and oxygen. No other peaks are evident. Therefore, it can be concluded that formation of complete solid solution has taken place in the fluorite host structure.

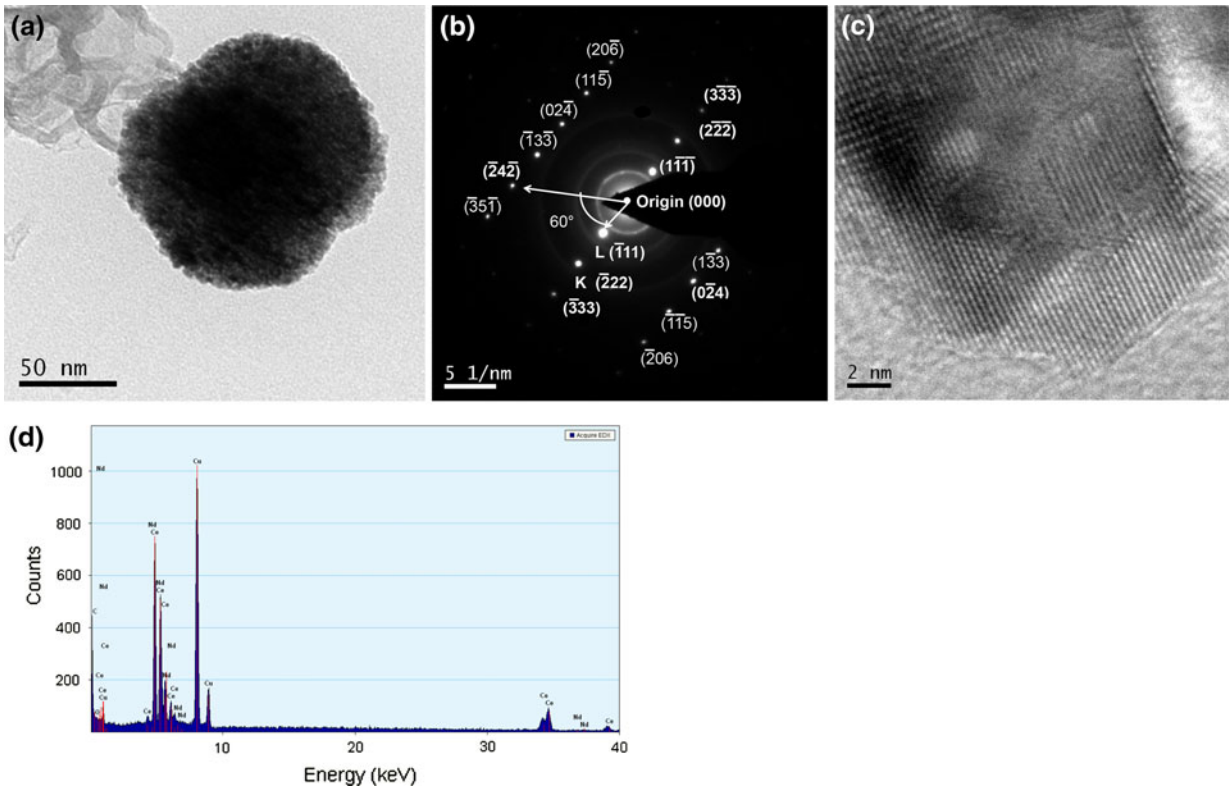


Fig. 7—(*a*) TEM image of ceria doped with 4 mol pct of $NdO_{1.5}$. (*b*) SAED pattern of the particle shown in (a). (*c*) HR pattern of the particle shown in (a). (*d*) EDX pattern of the particle shown in (a).

## IV. CONCLUSIONS

Nd-doped ceria powders with Nd concentration varying from 4 to 20 mol pct has been produced following the gel combustion route using UF as fuel. The cross-linking reaction, decomposition of stable gel structure, and crystallization occur consecutively at temperatures at 497 K, 524 K, and 587 K (224 °C, 251 °C, and 314 °C). The reaction becomes most vigorous during decomposition of the stable structure. The lattice parameter increases with Nd concentration, yet it deviates from Vegard's law. Crystallite size decreases with increasing dopant concentration. The particles were porous in nature and were mostly single crystalline, existing in a loosely agglomerated state. The size of the agglomerates increases with increasing dopant content.

## ACKNOWLEDGMENTS

The first author (M.B.) conveys her sincere thanks to CSIR for financial assistance through the grant of research associate position. Sincere thanks are also due to the Director, Central Glass and Ceramic Research Institute, Kolkata, India, for his encouragement. The help of service sections of CGCRI and other colleagues is gratefully acknowledged.

## REFERENCES

1. P. Patsalas, S. Logothetidis, and C. Metaxa: *Appl. Phys. Lett.*, 2002, vol. 81 (3), pp. 466–68.
2. http://www.nanophase.com/products/benefit.aspx?BenefitId=6.00.
3. P. Jasinski, T. Suzuki, and H.U. Anderson: *Sens. Actuators B*, 2003, vol. 95, pp. 73–77.
4. S. Tsunekawa, R. Sivamohan, T. Ohsuna, A. Kasuya, H. Takahashi, and K. Tohji: *Mater. Sci. Forum*, 1999, vols. 315–317, pp. 439–45.
5. K. Eguchi, T. Setoguchi, T. Inoue, and H. Arai: *Solid State Ionics*, 1992, vol. 52, pp. 165–72.
6. S. Patil, S.C. Kuiry, and S. Seal: *Proc. R. Soc. Lond. Ser. A*, 2004, vol. 460, pp. 3569–87.
7. S. Deshpande, S. Patil, S. Kuchibhatla, and S. Seal: *Appl. Phys. Lett.*, 2005, vol. 87 (13), p. 33113.
8. J.E. Spanier, R.D. Robinson, F. Zheng, S.W. Chan, and I.P. Herman: *Phys. Rev. B*, 2001, vol. 64, pp. 245407-1–245407-8.
9. T. Masui, T. Ozaki, K. Machida, and G. Adachi: *J. Alloys Compd.*, 2000, vol. 303, pp. 49–55.
10. S. Patil, S. Seal, Y. Guo, A. Schulte, and J. Norwood: *Appl. Phys. Lett.*, 2006, vol. 88 (24), p. 243110.
11. W.D. Kingery, H.K. Bowen, and D.R. Uhlmann: *Introduction to Ceramics*, Wiley, New York, 1976.
12. P.G. Harrison, A. Kelsall, and J.V. Wood: *J. Sol-Gel Sci. Technol.*, 1999, vol. 13 (1–3), pp. 1049–55.
13. A. Hartridge, A.K. Bhattacharya, R.E.D. Borkowski, and J.L. Hutchison: *J. Nanopart. Res.*, 2001, vol. 3 (5–6), pp. 431–39.
14. S.V. Chavan, M.D. Mathews, and A.K. Tyagi: *Mater. Res. Bull.*, 2005, vol. 40 (9), pp. 1558–68.
15. S. Omar, E.D. Wachsman, J.L. Jones, and J.C. Nino: *J. Am. Ceram. Soc.*, 2009, vol. 92 (11), pp. 2674–81.
16. H. Li, C. Xia, M. Zhu, Z. Zhou, and G. Meng: *Acta Mater.*, 2006, vol. 54, pp. 721–27.

17. K. Higashi, K. Sonoda, H. Ono, S. Sameshima, and Y. Hirata: *J. Mater. Res.*, 1999, vol. 14 (3), pp. 957–67.
18. B. Matović, J. Dukić, A. Devečerski, S. Bošković, M. Ninić, and Z.D. Mitrović: *Sci. Sinter.*, 2008, vol. 40 (1), pp. 63–68.
19. S.V. Chavan, P.U.M. Sastry, and A.K. Tyagi: *J. Alloy Compd.*, 2008, vol. 456 (1–2), pp. 51–56.
20. S. Bhaduri, S.B. Bhaduri, and E. Zhou: *J. Mater. Res.*, 1998, vol. 13, pp. 156–65.
21. V.V. Bedekar, S. Patra, A. Dutta, R.N. Basu, and A.K. Tyagi: *Int. J. Nanotechnol.*, 2010, vol. 7 (9), pp. 1178–87.
22. R.N. Basu, F. Tietz, E. Wessel, H.P. Buchkremer, and D. Stoever: *Mater. Res. Bull.*, 2004, vol. 39, pp. 1335–45.
23. M.W. Raja, S. Mahanty, P. Ghosh, R.N. Basu, and H.S. Maiti: *Mater. Res. Bull.*, 2007, vol. 42 (8), pp. 1499–506.
24. M. Biswas, K. Prabhakaran, N.M. Gokhale, and S.C. Sharma: *Mater. Res. Bull.*, 2007, vol. 42, pp. 609–17.
25. K. Prabhakaran, J. Joseph, N.M. Gokhale, S.C. Sharma R. Lal: *J. Am. Ceram. Soc.*, 2006, vol. 89 (7), pp. 2335–37.
26. J.C. Salamone: *Polymer Materials Encyclopedia*, vol. 11, CRC Press, Boca Raton, FL, 2000.
27. K.J. Saunnders: *Organic Polymer Chemistry*, Chapman and Hall, London, U.K., 1977.
28. B.D. Culity: *Elements of X-Ray Diffraction*, Addison-Wesley, Reading, MA, 1978.
29. G. Camina, L. Operty, L. Costa, and L. Trosarelli: *Thermal Analysis*, vol. II, M. Bernad, ed., Wiley, New York, 1992.
30. R.D. Shannon: *Acta Cryst. A*, 1976, vol. 32, pp. 751–67.
31. C.Y. Fong, W. Weber, and J.C. Phillips: *Phys. Rev. B*, 1976, vol. 14 (12), pp. 5387–91.
32. I. Yeriskin and M. Nolan: *J. Phys.: Condens. Mater.*, 2010, vol. 22 (13), p. 135004.
33. J.-F. Jerratsch, X. Shao, N. Nilius, H.-J. Freund, C. Popa, M.V. Ganduglia-Pirovano, A.M. Burow, and J. Sauer: *Phys. Rev. Lett.*, 2011, vol. 106, pp. 246801–1.
34. F. Wang, Y. Han, C.S. Lim, Y. Lu, J. Wang, J. Xu, H. Chen, C. Zhang, M. Hong, and X. Liu: *Nature*, 2010, vol. 463, pp. 1061–65.
35. M.C.A. Nono: *Mater. Sci. Forum*, 2006, vols. 530–531, pp. 461–66.
36. I.S. Altman, I.E. Agranovski, and M. Choi: *Appl. Phys. Lett.*, 2005, vol. 87, p. 053104.
37. J.W. Eddington: *Practical Electron Microscopy in Materials Science, Monograph 2*, MacMillan, Philips Technical Library, London, U.K., 1975.
38. C. Hammond: *The Basics of Crystallography and Diffraction, third edition, International Union of Crystallography*, Oxford Science Publications, Oxford, U.K., 2009.
39. M.V. Ganduglia-Pirovano, J.L.F. DaSilva, and J. Sauer: *Phys. Rev. Lett.*, 2009, vol. 102, p. 026101.